Electrochemical and Morphology of Corrosion Inhibition of C-Steel in 2 M HCl

4 authors, including:

Hala M Hassan
Beni Suef University
16 PUBLICATIONS **104** CITATIONS

Ahmed Mohammed Eldesoky
High Institute of Engineering &Technology (New Damietta), Egypt.
80 PUBLICATIONS **441** CITATIONS

Some of the authors of this publication are also working on these related projects:

Inhibition of C-steel corrosion. View project

Eco-friendly Corrosion inhibitors View project

Electrochemical and Morphology of Corrosion Inhibition of C-Steel in 2 M HCl

Y. Reda[1] · Hala. M. Hassan[2,3] · A. Attia[4,5] · A. M. Eldesoky[6]

Abstract

The main focus and novelty of this work is to use various concentrations of 2-((1E)-2-(1, 6-Dihydropyren-10-yl)vinyl) benzo[d]oxazole (Compound (I)) and 2-Styrylbenzo[d]oxazole (Compound (II)) as a source of corrosion inhibitors in order to prevent corrosion of C-steel in 2 M HCl. SEM technique EDX was utilized to look at the morphology of the shielded C-steel. The binding between benzo[d]oxazole assembled, & the receptor of 3hb5-oxidoreductase which is a breast cancer mutant and predicted using molecular docking. At 303 K, weight loss and electrochemical tests analysed this inhibitory action on corrosion of C-steel in 2 M HCl solution. As the temperature rises, the protective efficacy decreases marginally. IE likely to be lower in the following situations: Compound (I) > Compound (II).

Keywords Breast cancer · Adsorption · C-steel · Aggressive · DFT (Density Functional Theory)

1 Introduction

When evaluated to corrosive nature such as acidic media, the phenomena of corrosion are simply favoured on lesser noble metals. To remove scale and salts from C-steel surfaces, hydrochloric acid is widely employed [1]. Inhibitors are usually utilized to postpone the aggressive attack on the alloy due to the typical acidic corrosive solutions. [2–8]. Organic assemblies with electronegative and electron functional groups in triple or double bonds, are the principal active sites for adsorption [9–12]. The solution chemical composition; the potential electrochemical of both the solution-metal surface and the surface metal nature determine the manner of adsorption. [13–15] is a frequent goal of protection offered by corrosion scientists. At ambient temperature, IL compounds emerge as the best and smartest solvents [16–18]. Most features for inorganic and organic assemblies [19–25] include maximal thermal stability, elimination of vapour pressure, inflammability, non-coordinating yet excellent solvating ability, and good solubility [26]. Organic solvents are used as environmentally favourable alternatives [27]. It has been discovered that ILs based on pyridazinium, imidazolium, and pyridinium inhibit corrosion in certain alloys [28–42].

The main focus and novelty of this work is to use various concentrations of 2-((1E)-2-(1,6-Dihydro-pyren-10-yl)vinyl)benzo[d]oxazole (Compound (I)) and 2-Styrylbenzo[d]oxazole (Compound (II)) as a source of corrosion inhibitors in order to prevent corrosion of C-steel in 2 M HCl. The reason for using this concentration is that it is the same concentration in which carbon steel corrodes in petroleum installations and industrial media, i.e. its imitation of the natural erosion medium found in various fields of industry and oil installations. Determining the parameters of thermodynamic activation. SEM and EDX methods were used to examine the picture of shielded C-steel. The use of a quantum chemical technique based on DFT was employed to acquire a better

✉ Y. Reda
  ysyy5@hotmail.com

1   Canal High Institute of Engineering and Technology, Suez, Higher Technological Institute, 10Th Ramadan (HTI), Cairo 11722, Egypt

2   Textile Technology Department, Faculty of Technology and Education, Beni-Suef University, Beni Suef, Egypt

3   Chemistry Department, Faculty of Science, Jazan University, jizan, Kingdom of Saudi Arabia

4   Department of Chemistry, Faculty of Science, Mansoura Univrsity, Mansoura, Egypt

5   Faculty of Science and Arts, Chemistry Department, Najran University, Najran, Kingdom of Saudi Arabia

6   Chemical Engineering Department, High Institute of Engineering &Technology, New Damietta, Egypt

understanding of the connection between IE percent and molecular atoms of benzo[d]oxazole derivatives, as well as the analysis of quantum chemical parameters.

2 Material and Methods

2.1 Measurements

The Docking Server [43] is used to simulate and measure the ligand–protein pair-wise reaction energy during the docking process. The MMFF94 Force field was used to reduce the energy of a ligand molecule using the Docking Server. The partial charges of Gasteiger were added to the compounds' atoms (I) and (II). Rotatable bonds were created by combining non-polar hydrogen atoms. Docking calculations were performed on the protein models of compounds (I) and (II) [44]. The Auto Dock parameter distance and set reliance on dielectric functions were consistently employed in the electrostatic and van der Waals terms analyses.

2.2 Chemical Composition Materials

Corrosion calculations were done using C-steel. Si (0.30), (0.045) P, Mn (0.53), S (0.055), (0.20) C, and iron is the rest. The corrosive medium was made of (2 M HCl). 2-((1E)-2-(1, 6-Dihydropyren-10-yl)vinyl)benzo[d]oxazole (Compound (I)) and 2-Styrylbenzo[d]oxazole (Compound (II)) are benzo[d]oxazoles that have been constructed. As shown in Table 1 [45].

2.3 Corrosion Test

2.3.1 Weight Loss Tests

C-steel coins with a spacing of $20 \times 20 \times 2$ ml were pounded with grades of paper emery; acetone was used to clean the coins, rinsed with distilled water and drained among filter papers. After being precisely weighed, the coins were placed in a beaker containing 100 ml of 2 M HCl and kept at 30 ± 0.1 °C, in the presence and absence of various doses of benzo[d]oxazole derivatives. After varied immersion times, the C-steel coins were retrieved, cleaned with bi-distilled water, dried, and weighed again. To calculate R (the rate of corrosion in mmy-1) the following formula is used (1) [46]:

$$R = \frac{(8.75 \times \text{Weightloss in gram} \times 104)}{DAT} \tag{1}$$

where T is the time of exposure in hours, A is the target area in square metres, and D is the iron density in grammes per cubic metre. The protection efficiency (percent IE) and () were calculated using the following Eq. (2):
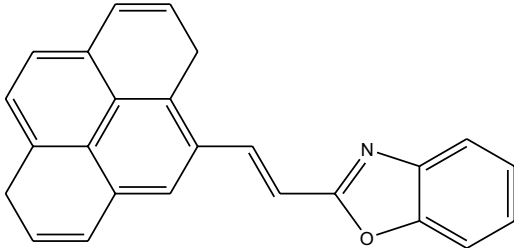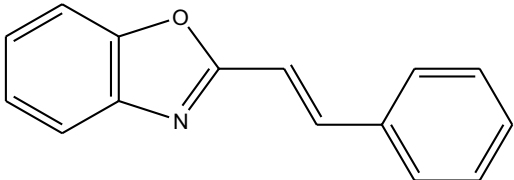
$$\%\text{IE} = 100 \times \theta = 100 \times \left[\frac{(R^* - R)}{R^*} \right] \tag{2}$$

In the presence and absence of inhibitors, the rates of corrosion of C-steel are R and R^*, respectively.

2.3.2 Electrochemical Methods

These calculations were performed using a Gamrypotentiostat/ZRA/galvanostat (PCI300/4model) in an imitative three electrodes thermostatic cell assembly. A calomel electrode

Table 1 Chemical structure, name, molecular weight, and a molecular formula of inhibitors

Compound No	Structure	Name	Mol. Wt./M. Formula
(I)		2-((1E)-2-(1,6-Dihydropyren-10-yl) vinyl)benzo[d]oxazole	347/$C_{25}H_{17}NO$
(II)		2-Styrylbenzo[d]oxazole	221/$C_{15}H_{11}NO$

(SCE) and a platinum foil (Pt) were utilised continually as reference and counter electrodes. The C-steel electrodes were 10×10 ml in size and were welded together using Cu wire from a single location for electrical coupling. All of the results were obtained at 30 °C minus 0.1 °C. After the supplied steady-state (30 min) and (OCP) after 15 min of electrode immersion in the test solution, the Potentiodynamic. The open circuit potential (OCP) is the potential of the working electrode relative to the reference electrode when no potential or current is being applied to the cell. When a potential is applied relative to (OCP), the system measures the open circuit potential before turning on the cell, then applies the potential relative to that measurement. For example, if the initial potential is set to $+ 100$ mV vs. (OCP) in the software and the measured open circuit potential is $+ 300$ mV, then the initial potential will be set to $+ 400$ mV. EIS and EFM tests were conducted using similar behaviours as system of Gamry framework based on ESA400. Gamry provided EIS300 software for EIS tests and EFM140 software for EFM calculations; data summing was done on a computer. For sketching, fitting, and graphing values, Echem Analyst 5.5 was utilised. At each corrosion potential, EIS measurements were taken using a frequency range of 100 kHz to 10 MHz and a 5 mV amplitude of ac signals. EFM makes use of two frequencies: 2 and 5 Hz.

2.3.3 Morphology

The C-steel surface was generated by immersing coins in 2 M HCl for three days without and with different quantities of benzo[d]oxazole derivatives, such as 2-((1E)-2-(1,6-Dihydropyren-10-yl)vinyl)benzo[d]oxazole (Compound (I)) and 2-Styrylbenzo[d]oxazole (Compound (II)), the coins were gently washed with distilled water, thoroughly dried, and put in the spectrometer. A diffractometer X-ray Philips (pw-1390) with a Cu tube was used to test the corroded C-steel surfaces (SEM, JSM-T20, JOEL, Japan).

2.3.4 Conceptual Research

Version 4.4 in Material Studio was used to do quantum chemistry calculations.

3 Results and Discussion

3.1 Weight Loss Method

The weight loss time curves for corrosion of C-steel in 2 M HCl in the absence and presence of different concentrations of compound are shown in tabure 1. (I). Table 2 demonstrates that as the concentration of benzo[d]oxazole derivatives increase from 1×10^{-6} to 11×10^{-6} molar, the protection

Table 2 Weight loss technique at 1 h, immersion in acidic liquid at 30 ± 0.1 °C, percent IE variation with different benzo[d]oxazole compounds and their molar concentrations

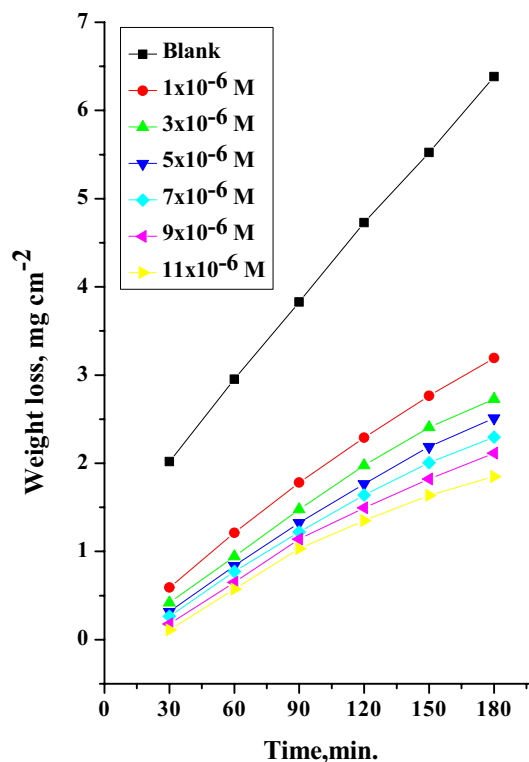| Conc. (M)	(%IE)	
	(I)	(II)
1×10^{-6}	51.6	44.2
3×10^{-6}	58.2	52.1
5×10^{-6}	62.7	54.5
7×10^{-6}	65.3	56.9
9×10^{-6}	68.4	58.3
11×10^{-6}	71.5	60.4

Fig. 1 Weight loss time curves for C-steel corrosion in the absence and presence of different concentrations of compound (I) at 30 ± 0.1 °C

efficacy improves. At concentration, the best (percentage IE) was provided (11×10^{-6} M). Because the least (percent IE) is combined with compound (II), percent IE likely to be lower in the following situations: Compound (I) > Compound (II) (See Fig. 1).

3.1.1 Adsorption Isotherm

Adsorption sheds light on the corrosion prevention process by simulating the reaction between the adsorb molecules and the electrode surface. The Temkin isotherm model assumes that the adsorption heat of all molecules decreases linearly with the increase in coverage of the adsorbent surface, and that adsorption is characterized by a uniform distribution of

binding energies, up to a maximum binding energy. Using the Temkin equation yields [47]:

$$\theta = \frac{2.303}{a \log c} + \frac{2.303}{a \log K_{ads}} \quad (3)$$

where K_{ads} stands for the equilibrium adsorption constant and C stands for the inhibitor concentration. A straight line was drawn to represent the relationship between versus log C. (obtain in Fig. 2). The intercept is used to calculate Kads. The following sources were also used to obtain goads:

$$log K_{ads} = -log 55.5 - \Delta G^o{}_{ads}/2.303RT \quad (4)$$

The universal constant of gases is R, the mole/liter concentration of water in solution is 55.5, and the Kelvin temperature is T [48]. The K_{ads} data is obtained from Table 3 and is used to calculate the percent IE [K (I) > K (II)]. Due to the forming structure on the surface of C-steel, this result inverts the capability improvement [49].

3.1.2 Parameters of Kinetic Activation

The activation energies (Ea*) for C-steel corrosion in 2 M HCl in the absence and presence of varying quantities of benzo[d]oxazoles derivatives were calculated by Arrhenius-equation [50]:

Table 3 Parameters K_{ads}, $\Delta G_{ads.}$, and later interaction parameter (a) for benzo[d]oxazole derivatives at 30 ± 0.1 °C

Inhibitors	Temkin isotherm		
	a	K_{ads}, M^{-1}	$-\Delta G_{ads}$, kJmol^{-1}
Compound (I)	59.8	1.21	10.53
Compound (II)	77.9	1.15	10.48

$$\log k = \log A - E_a * /2.303RT \quad (5)$$

where k stands for constant rate, A stands for factor pre-exponential, Ea* stands for corrosion activation energy, T stands for absolute temperature, and R stands for constant gas universal. Figure 3 shows Arrhenius curves of 1/T vs.log k for C-steel in 2 M HCl without and with varied amounts of chemical (I). The variation follows a straight line. Ea* data was calculated using the slope of these lines, which was then documented in Table 4. The energy barrier for corrosion improves when Ea* rises due to the addition of inhibitor concentrations (I, II). The whole corrosion process is carried out by surface reaction because the activation energy of the corrosion process is more than 20 kJ mol^{-1}[51]. The equation transition state (6) was given by performance for C-steel corrosion in acidic medium:

Fig. 2 Temkin isotherm curve for C-steel in 2 M HCl with various inhibitor concentrations at 30 ± 0.1 °C
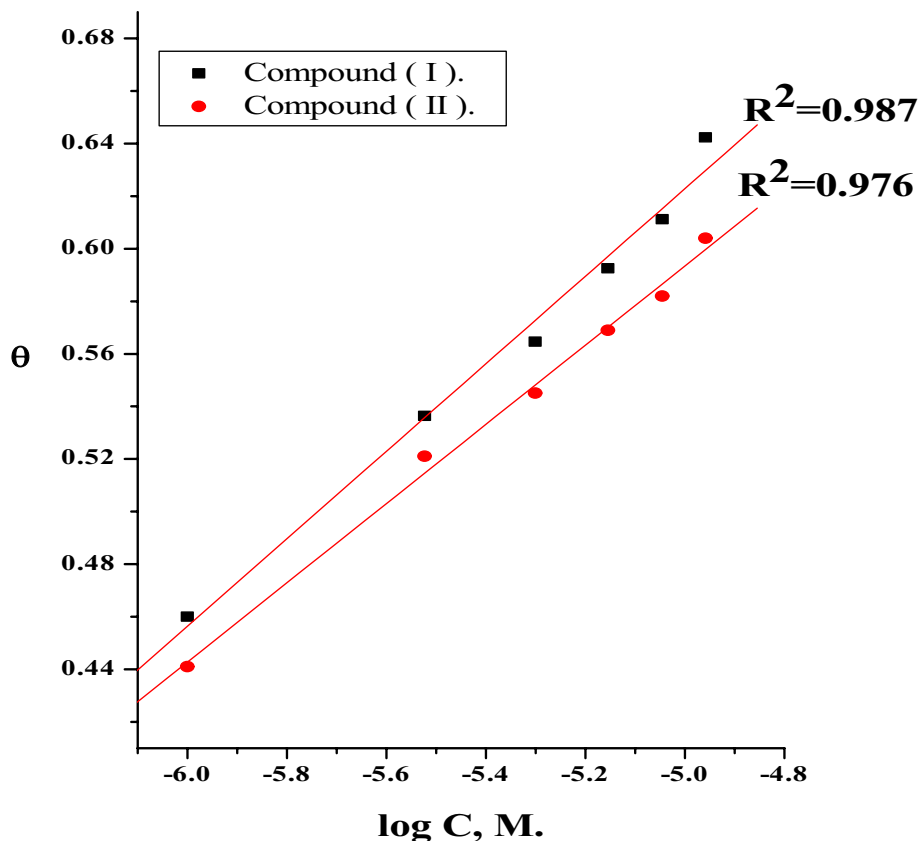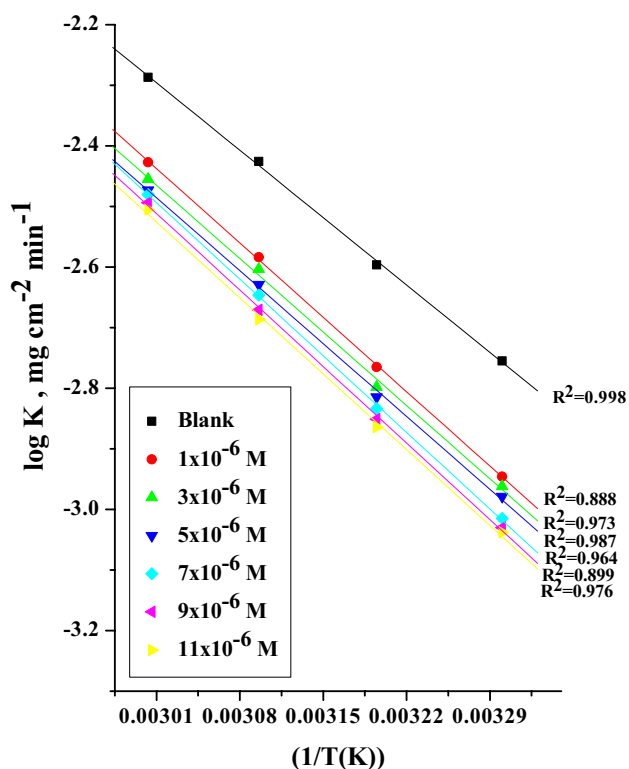
Fig. 3 Log (corrosion rate) vs. (1/T) curves for C-steel corrosion in 2 M HCl in the absence and presence of different concentrations of inhibitor (I)

$$K = (TR/Nh)e^{(\Delta S*/R)}e^{(-\Delta H*/RT)} \tag{6}$$

Avogadro's number is N, while Planck's constant is h. A plot of 1/T against log k/T yielded straight lines for C-steel

Table 4 Shows the kinetic characteristics of C-steel corrosion in 2 M HCl in the absence and presence of various amounts of the organic chemicals studied (I, II)

Inhibitor	Conc., M	Ea*, kJ mol^{-1}	ΔH*, kJ mol^{-1}	-ΔS*, J mol^{-1} K^{-1}
	Blank	20.9	17.8	155.1
Compound (I)	1×10^{-6}	28.4	25.6	136
	3×10^{-6}	31	28.6	126.5
	5×10^{-6}	33.1	30.5	121.3
	7×10^{-6}	33.8	31.3	119.4
	9×10^{-6}	34.7	32.2	117.1
	11×10^{-6}	35.3	32.8	116
Compound (II)	1×10^{-6}	26.3	23.6	141.2
	3×10^{-6}	28.7	26.9	134.4
	5×10^{-6}	29.6	27.1	131.3
	7×10^{-6}	29.7	27.2	131.1
	9×10^{-6}	29.8	27.4	130.7
	11×10^{-6}	30.2	27.7	130.2

liquefaction in 2 M HCl with and without inhibitor doses, as illustrated in Fig. 4. (I).

Using the lines slopes = -– H*/2.303R and the intercept = log RT/Nh + (S*/2.303R), the values of H* and S* were measured and documented in Table 4. According to these findings, the presence of the tested chemicals raises Ea* values, lowering the C-steel corrosion rate. These conclusions are based on the fact that the tested compounds increase Ea* of C-steel liquefaction by generating a charge transfer barrier on the alloy surface via adsorption. The endothermic type of the C-steel liquefaction process is inverted when the enthalpies have a positive sign. The corrosion process must comprise a gaseous reaction with a simple hydrogen reaction evolution and a decreased total volume of reaction since the Ea* values are bigger than the corresponding H* data [52]. The data for S* are higher and negative in the absence and presence of various concentrations of the tested compounds, indicating that the activated complex in the rate-determining step associates rather than dissociates, implying that there is less disordering when going from reactants to the activated complex [53, 54].

3.2 Potentiodynamic Characterization

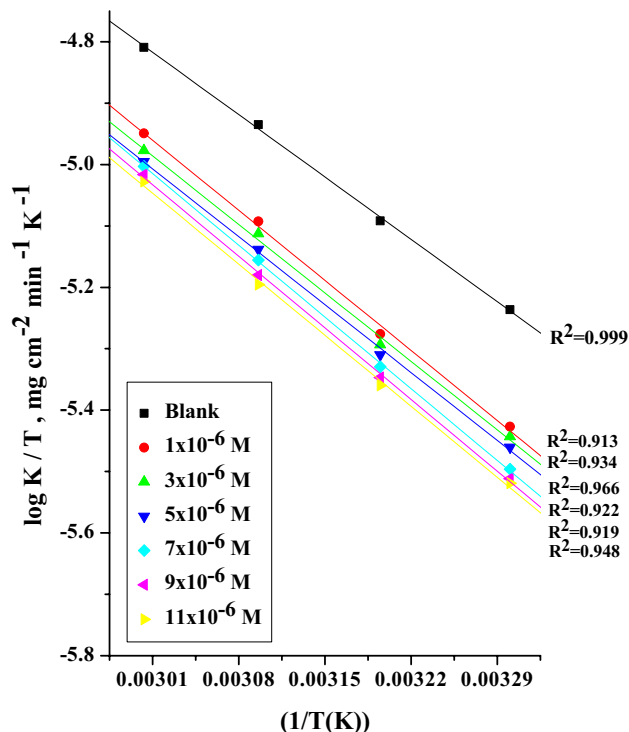Figure 5 shows the polarisation curves of C-steel in an acidic solution with and without various quantities of

Fig. 4 Log (corrosion rate/T) vs. (1/T) curves for C-steel corrosion in 2 M HCl in the absence and presence of different concentrations of inhibitor (I)

Fig. 5 Potentiodynamic Polarization curves for the C-steel corrosion in 2 M HClin the absence and presence of different concentrations of inhibitor (I) at 30±0.1 °C
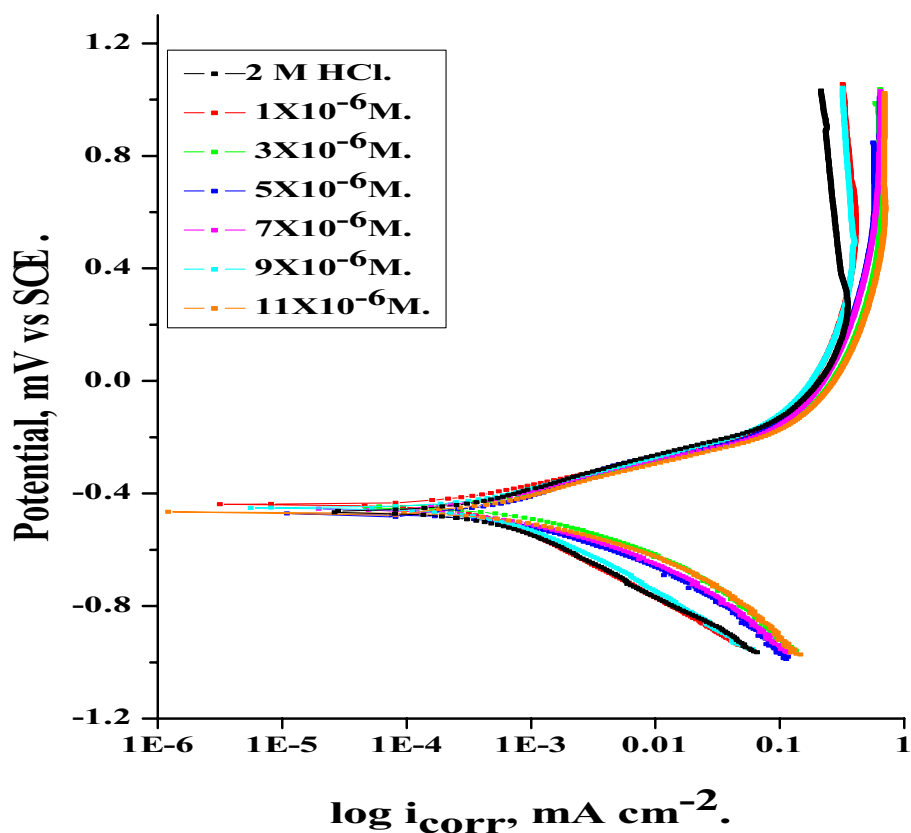
chemical. (I). It shows how adding investigated benzo[d] oxazole derivatives affected both the anodic and cathodic reactions, with the percent IE increasing as the inhibitor concentration increases, but the cathodic reaction is more protective, indicating that adding benzo[d]oxazole derivatives break down the C-steel anodic liquefaction while also preventing the cathodic site. The benzo[d]oxazole compounds studied operate as mixed inhibitors. Table 5 shows that after adding inhibitors, the icorr decreases and the percent IE increases as the inhibitor concentration increases. The following formula was used to calculate the percent IEp:

Table 5 Shows the effects of organic compound concentrations (I, II) on (i_{corr}), (E_{corr}), (βa & βc), and (% IE) for C-steel at 30±0.1 °C

Conc., M	i_{corr} X 10^{-4}, mA cm $^{-2}$	$-E_{corr}$ mV vs (SCE)	βa X 10^{-3}, mV dec^{-1}	βc X 10^{-3}, mV dec^{-1}	% IE
Blank	8.13	495	136	132	—
Compound (I)					
1×10^{-6}	3.12	467	115	107	61.6
3×10^{-6}	2.79	439	73	10	65.6
5×10^{-6}	2.13	460	102	101	73.8
7×10^{-6}	1.94	454	191	106	76.1
9×10^{-6}	1.92	470	95	86	76.3
11×10^{-6}	1.77	453	40	41	78.2
Compound (II)					
1×10^{-6}	4.67	482	123	121	42.5
3×10^{-6}	4.13	490	103	102	49.2
5×10^{-6}	4.01	477	117	115	50.6
7×10^{-6}	3.49	459	103	104	57.0
9×10^{-6}	3.01	478	112	67	62.9
11×10^{-6}	2.94	499	108	98	63.8

$$\% \ IE_p = 100 \times \left[i^o_{corr} - i_{corr} / i^o_{corr} \right] \qquad (7)$$

The inhibited and uninhibited corrosion current densities are i_{corr} and $i^o corr$, respectively.

In both anodic and cathodic applications, inhibitors adsorbed function by simply obstructing the active centre, as shown in Table 5.

The adsorption inhibitors reduce corrosion surface area while having no effect on the corrosion process of C-steel, and only inactivation exposes a portion of the C-steel surface to the aggressive solution [55, 56]. Compound (I) > Compound (II). According to mass reduction techniques, the ability to block 2 M HCl rises from (I) to (II) because of a free pair of electrons in the other

molecular structure, electrons on aromatic nuclei, the N atom, and inversion (II).

3.3 EIS

Experiments were carried out with and without inhibitors in acid solution at 30 ± 0.1 °C. Figure 6 shows an insert for the equivalent circuit model of the current corroding system's metal/electrolyte interface, where Rs, Rct, and CPE stand for solution resistance, charge transfer resistance, and constant phase element, respectively, representing the interface's double-layer capacitance (Cdl). Nyquist plots show a typical example of EIS data generated for chemical (I) [as the most effective inhibitor] Fig. 7

The impedance spectra are of the Nyquist semicircle type, with no trace of diffusive contribution to the total impedance

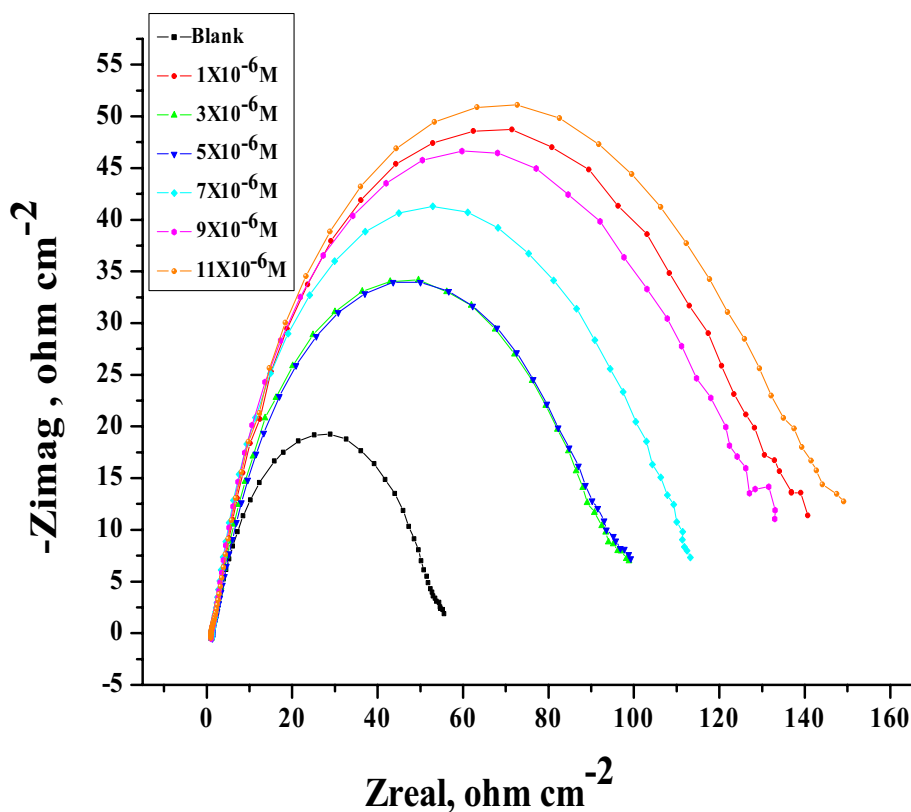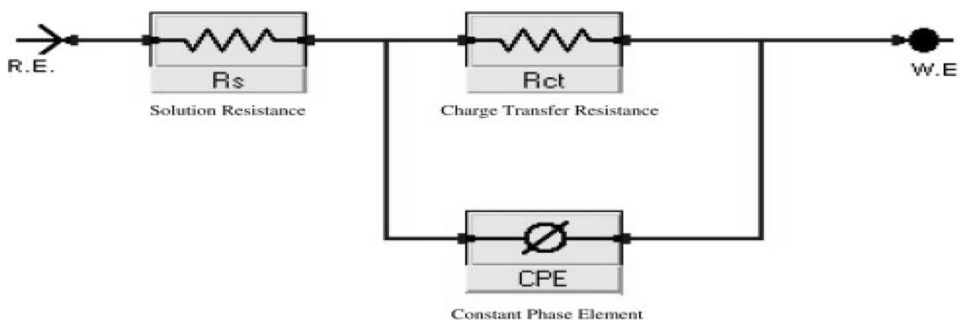**Fig. 6** Equivalent circuit model utilized to fitting EIS data

Fig. 7 EIS Nyquist plots for C-steel corrosion in 2 M HCl in the absence and presence of different concentrations of inhibitor (I) at 30 ± 0.1 °C

(Z), indicating that charge transfer is the primary control mechanism for corrosion and that the presence of inhibitor has no influence on this mechanism [57, 58]. Frequency dispersion was responsible for a little degree of distortion in the plots [62, 63]. The diameters of the capacitive loops grow in the presence of inhibitors, reflecting the amount of corrosion inhibition, rather than a decrease in the capacity of the double-layer (Cdl), as indicated by Eq. (8):

$$Cdl = Yo \, \omega n - 1/ \sin \left[n \left(\pi/2 \right) \right] \quad (8)$$

where ω=2πfmax, Yo=CPE magnitude, fmax=frequency of imaginary compound of the maximum EIS and n=factor utilized among 0.50 and 1.0.

According to the EIS parameters, the size of the semicircles grows as the concentration of the investigated inhibitors increases. This indicates that when inhibitor concentrations rise, the oxide layer's polarisation resistance Rct rises, resulting in a reduction in corrosion rate [64–66]. Surface roughness and inhomogeneity are terms used to describe this capacitive semicircle, which is linked to dielectric properties and the thickness of the barrier oxide layer. It's vital to ensure that when inhibitor concentrations grow, C_{dl} levels fall. Because deposited inhibitor molecules eventually replace water molecules in the double layer, an adherent film forms on the metal surface, reducing the metal solution interface's local dielectric constant [67]. (Rct+Rs) corresponds to the high-frequency limitations. The charge transfer reaction's kinetic response is shown in the low-frequency contribution [68, 69]. Table 6 shows that the efficiency of inhibition (percent IE EIS) of these compounds follows the same pattern as before: (I) > (II). The Rct value from the next eqn was used to calculate the percent IE. 9) [70]:

$$\%IE_{EIS} = 100 \times \left[1 - \frac{R^o_{ct}}{R_{ct}} \right] \quad (9)$$

The charge-transfer resistance statistics in the presence and absence of inhibitor are represented by Rct and Roct, respectively [71, 72].

3.4 EFM

EFM testing indicate that it is a viable choice for corrosion online calculation [73]. Figure 8 shows the EFM with varied chemical concentrations (I). For other compounds, the same plots were used.

The harmonic and intermodulation bands are plainly visible and outnumber the background noise by a large margin. The "activation" model and the perfect control diffusion of the cathodic process were employed to treat EFM data. For the second, a set of three non-linear equations was built, assuming that the corrosion potential does not vary according to the polarisation of the electrode operating [74].

The value in Table 7 shows that adding any one of the tested compounds to the acidic medium at a particular concentration reduced icorr, indicating that these compounds prevent C-steel corrosion in 2 M HCl via adsorption. Because the causality factors acquired during various testing are essentially equivalent to the theoretical data, the computed data are very good and of the highest quality (2 and 3). As indicated in Eq. (10), raising the inhibitor concentration improves the % IE$_{EFM}$ [75]:

$$\%IE_{EFM} = 100 \times [1 - (i_{corr}/i\circ_{corr})] \quad (10)$$

Corrosion current densities in the presence and absence of inhibitors are denoted by icorr and iocorr, respectively.

Table 6 EIS parameters for C-steel in 2 M HCl in the absence and presence of different concentrations of benzo[d]oxazole compounds (I, II) at 30±0.1 °C in the absence and presence of different concentrations of benzo[d] oxazole compounds (I, II)

| Compound No	Conc., M	R_S, Ωcm^2	Y_o, ×10^{-6}μΩ^{-1}s^n	n X 10^{-3}	R_{ct}, Ω cm^2	C_{dl} X 10–4, μFcm^{-2}	%IE
Compound (I)	Blank	1.10	115.7	796.6	53.77	1.80	—
	1×10^{-6}	1.21	443.8	774.8	96.60	1.56	44.3
	3×10^{-6}	1.14	445.0	773.9	97.64	1.55	44.9
	5×10^{-6}	1.34	468.3	761.9	111.30	1.49	51.6
	7×10^{-6}	1.33	456.8	770.1	130.80	1.44	58.8
	9×10^{-6}	1.19	447.5	771.1	147.00	1.43	63.4
	11×10^{-6}	1.36	446.7	778.1	193.00	0.48	72.1
Compound (II)	1×10^{-6}	1.27	341.6	887.6	57.37	2.04	6.3
	3×10^{-6}	1.56	219.5	899.0	58.07	1.34	7.4
	5×10^{-6}	1.50	303.3	897.4	60.36	1.31	10.9
	7×10^{-6}	1.81	395.7	851.8	60.95	1.26	11.8
	9×10^{-6}	2.21	260.3	885.3	85.70	1.19	37.3
	11×10^{-6}	2.45	111.9	868.4	167.70	0.65	67.9
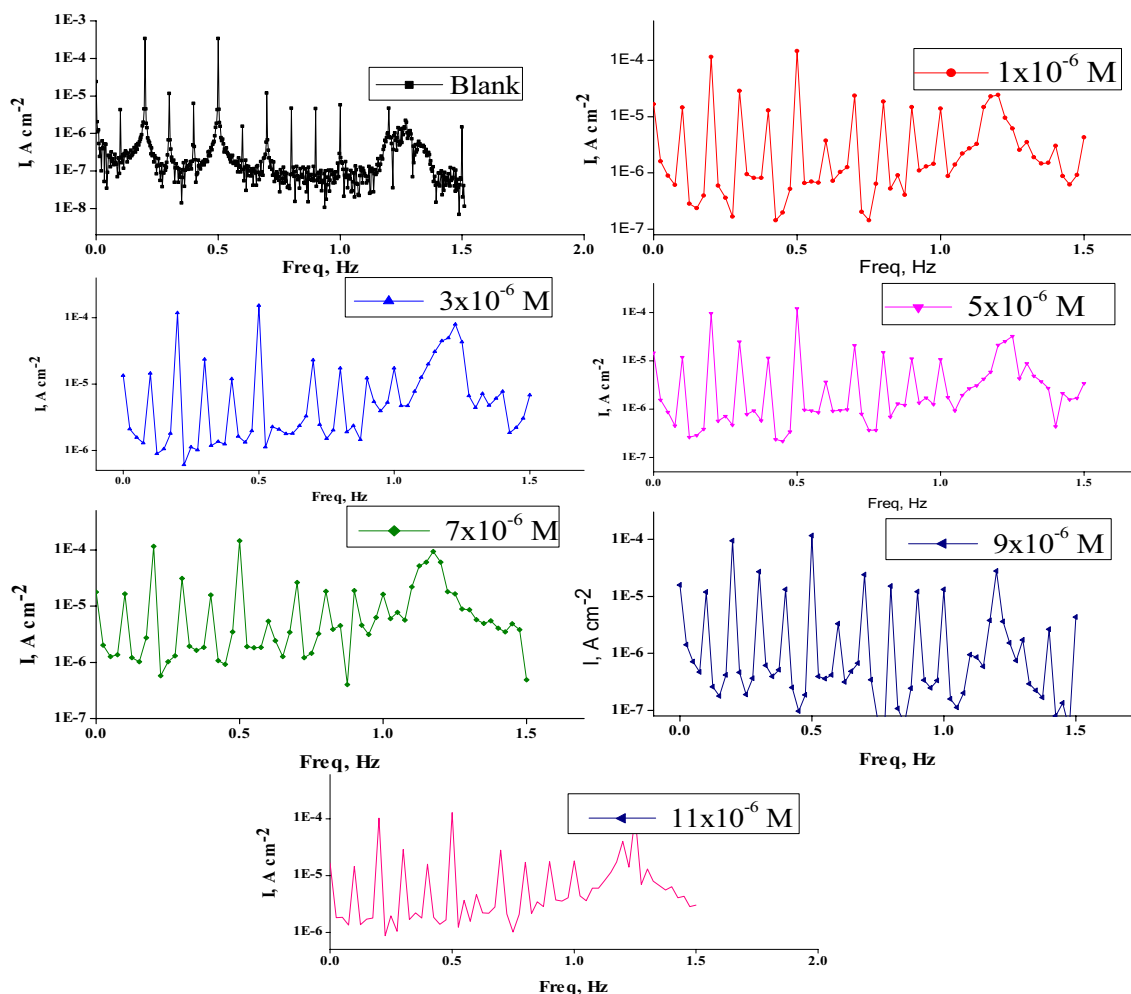
Fig. 8 EFM spectra for C-steel corrosion in 2 M HCl in the absence and presence of different concentrations of inhibitor (I) at 30 ± 0.1 °C

Table 7 EFM parameters testing for C-steel in 2 M HCl in the absence and presence of different concentrations of benzo[d]oxazole compounds (I, II) at 30 0.1 °C in the absence and presence of different concentrations of benzo[d]oxazole compounds (I, II)
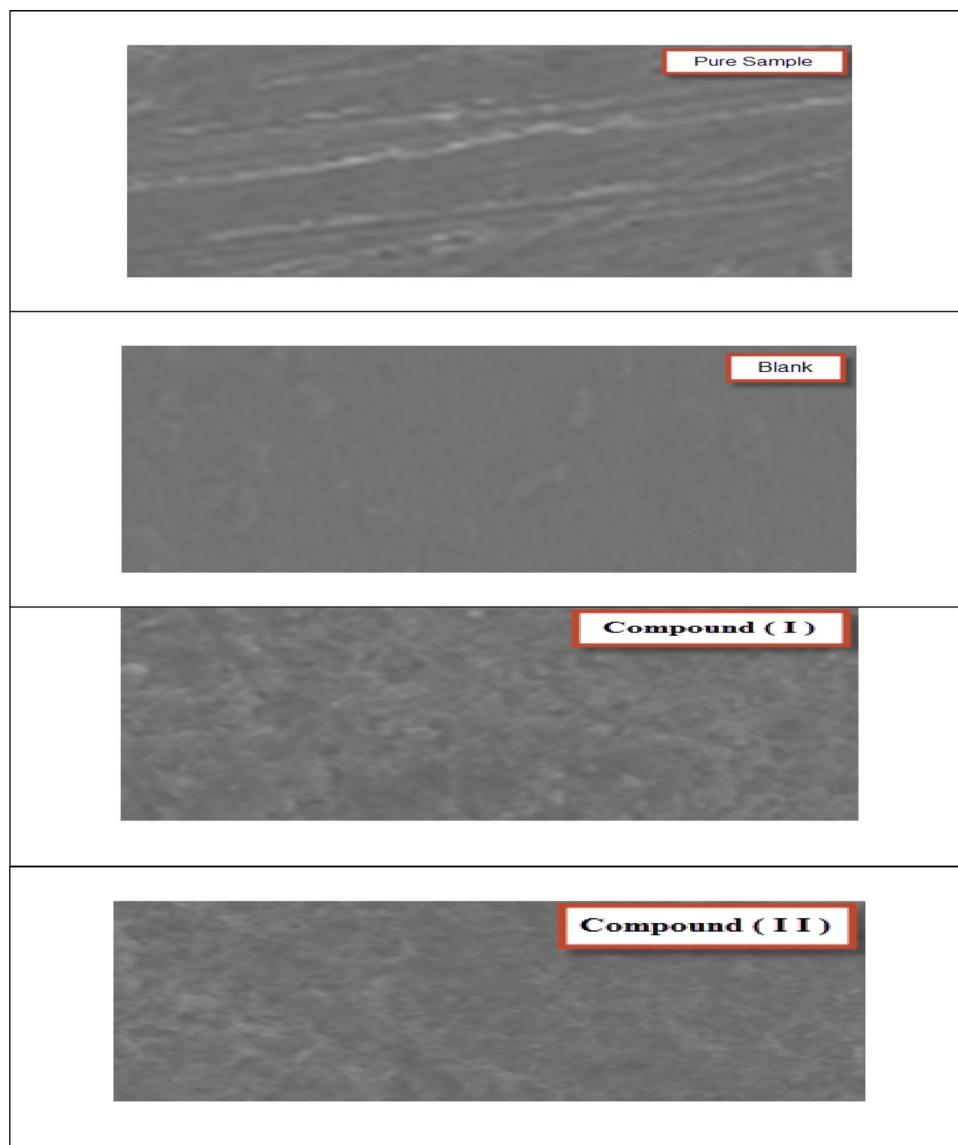
Compound No.	Conc., M	i_{corr}, μA cm^2	βa X 10^{-3}, mV dec^{-1}	βc X 10^{-3}, mV dec^{-1}	CF-2	CF-3	%IE
Compound (I)	Blank	128.4	29.02	40.65	2. 03	2.88	–
	1×10^{-6}	64.11	28.03	42.09	2	3.04	50.07
	3×10^{-6}	58.22	25.7	34.74	1.89	3.02	54.66
	5×10^{-6}	54.05	27.3	42.77	1.87	2.96	57.9
	7×10^{-6}	50.55	22	32.98	1.93	3.07	60.63
	9×10^{-6}	48.23	26.09	42.09	1.99	3	62.44
	11×10^{-6}	47.44	23.1	36.65	1.87	3.1	63.05
Compound (II)	1×10^{-6}	82.1	30,74	43	1.96	3.12	36.06
	3×10^{-6}	80.33	23,67	38.01	2.02	2.98	37.44
	5×10^{-6}	78.03	29.89	39.56	2.03	2.79	39.23
	7×10^{-6}	77.21	27.55	36.84	2.07	3.01	39.87
	9×10^{-6}	75.34	29.05	45.32	2.11	3.01	41.32
	11×10^{-6}	67.54	27.89	36.99	1.89	2.94	47.4

The order of protection adequacy given from this test is Compound (I) > Compound (II).

3.5 SEM

Figure 9 shows the micrographic results for C-steel coins after 3 days of immersion with and without 11×10^{-6} M of benzo[d]oxazole derivatives. In the blank sample, corrosion attacks on C-steel surfaces are severe. It's worth noting that the C-steel form changes considerably when the substance is present in the solution. The benzo[d]oxazole adsorption on the surface fused with the passive film to block the active site on the surface, resulting in the formation of a film that is scattered haphazardly throughout the entire C-steel surface.

3.6 EDX

After 3 days of immersion in the inhibited and absence of 2 M HCl, EDX was used to analyse the presence of components on the surface of C-steel. Only Iron and Oxygen were found in the EDX tests, indicating that only ferric oxide was used to make the coating film. Given the EDS analysis of C-steel alone and the presence of 11×10^{-6} M of benzo[d]oxazole compounds, portrays from Fig. 10.

The presence of Carbon is indicated by the spectra given in the appending lines (owing to the carbon of benzo[d]oxazole derivatives). The O and C atoms adhered to the coins as a result of these values. The absence of C and O signals on the C-steel outer surface introduced to uninhibited HCl indicates that this layer is entirely due to the inhibitor. The distribution of elements is seen in Table 8.
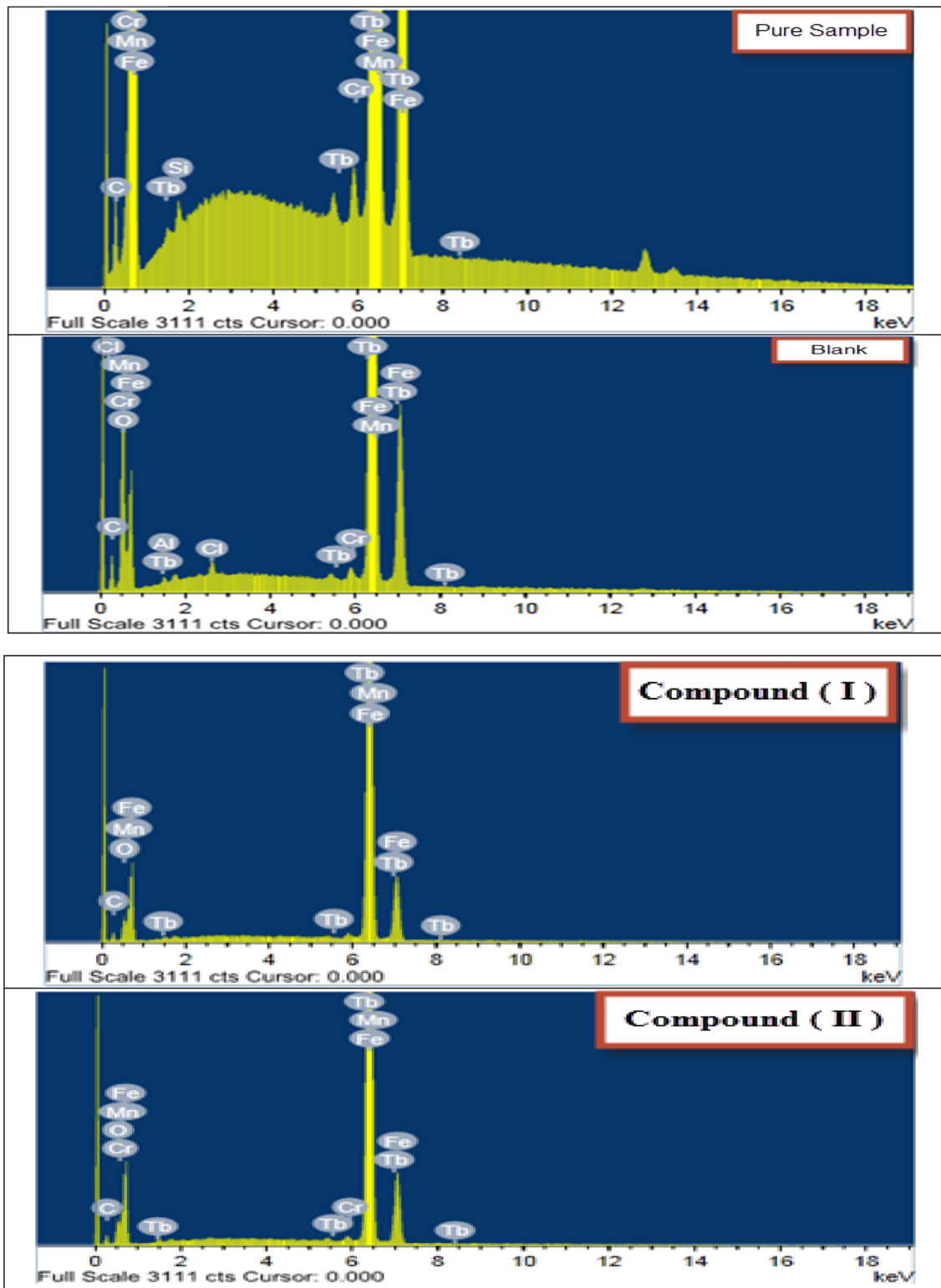

Fig. 9 SEM image of C-steel after immersion in $11 \times 10{-6}$ M benzo[d]oxazole derivatives for 3 days in the absence and presence of benzo[d]oxazole derivatives

Fig. 10 EDX analysis of C-steel solution after 3 days of immersion in the presence or absence of 11×10^{-6} M benzo[d]oxazole derivatives

3.7 Theoretical Research

The chemical orbital diagrams and Mulliken charges of benzo[d]oxazole derivatives are depicted in Fig. 11.

To acquire a better understanding of the experimental data, the theoretical analysis was confined to neutral forms.

Table 8 shows the weight percent of C-steel after 3 days in the presence and absence of 11×10^{-6} M Benzo[d]oxazole derivatives.

(Mass %)	Carbon	O	Si	Al	Cr	Mn	Fe	Tb	Cl
Pure Sample	6.78	–	0.28	0.29	0.22	0.47	87.53	4.43	–
Blank	10.99	21.58	–	0.30	0.16	0.34	62.75	–	0.33
Compound (I)	10.56	7.11	–	–	0.23	0.44	78.17	3.49	–
Compound (II)	10.23	7.14	–	–	0.17	0.43	78.16	3.87	–

Fig. 11 Molecular orbital plots of benzo[d]oxazole derivatives under investigation
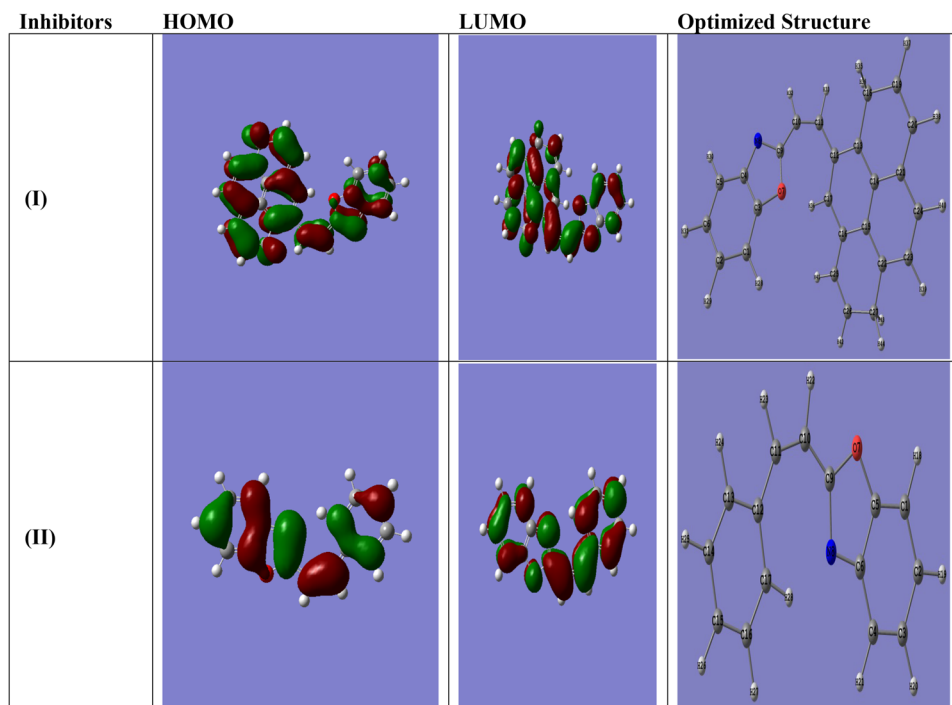
Table 9 shows the quantum chemistry results for benzo[d]oxazole derivatives

Factors	Compound (I)	Compound (II)
$-E_{HOMO}$ (a.u)	0.28682	0.30403
$-E_{LUMO}$ (a.u)	0.18142	0.13892
ΔE (a.u)	0.105	0.165
η (a.u)	0.053	0.083
σ (a.u)$^{-1}$	18.975	12.113
$-Pi$ (a.u)	0.234	0.221
χ(a.u)	0.234	0.221

The energies of (ELUMO) and (EHOMO) and (E) are measured and recorded as quantum compound lead to data in Table 9. The greater or lower the -ve EHOMO is connected to inhibitor, and the higher the trend of supplying electrons to the metal's empty orbital, the better the corrosion protection efficiency Furthermore, the lower the ELUMO, the easier it is to get electrons from the surface of C-steel [76, 78]. Due to adsorption on the C-steel surface and subsequent presence of the higher percent IE, the ΔE specified

by the four methods in the circumstance of substance (II) is lower than (I), which improves the hypothesis that (I) molecule will take in more excellent on C-steel surface than compound (II), which improves the hypothesis that C-steel surface is more molecule-absorbent than compound (II). The increase in E_HOMO from compound (I) to compound (II) aids in adsorbing and inhibiting by facilitating transport through the adsorbed layer. Perfect corrosion inhibitors are said to be made from organic compounds that not only supply electrons to the C-steel's empty orbital, but also gain electrons free from the metal [79]. These results are confirmed by quantum calculations.

3.8 Molecular Docking

Computer drug design relies heavily on molecular docking [80, 81]. The goal of molecular docking is to mimic the process of molecular recognition. The goal of molecular docking is to get an optimum confirmation for both drug and protein, with comparable results, such that the total system's free energy is as low as possible. We employed molecular docking to connect benzo[d]oxazole derivatives to the
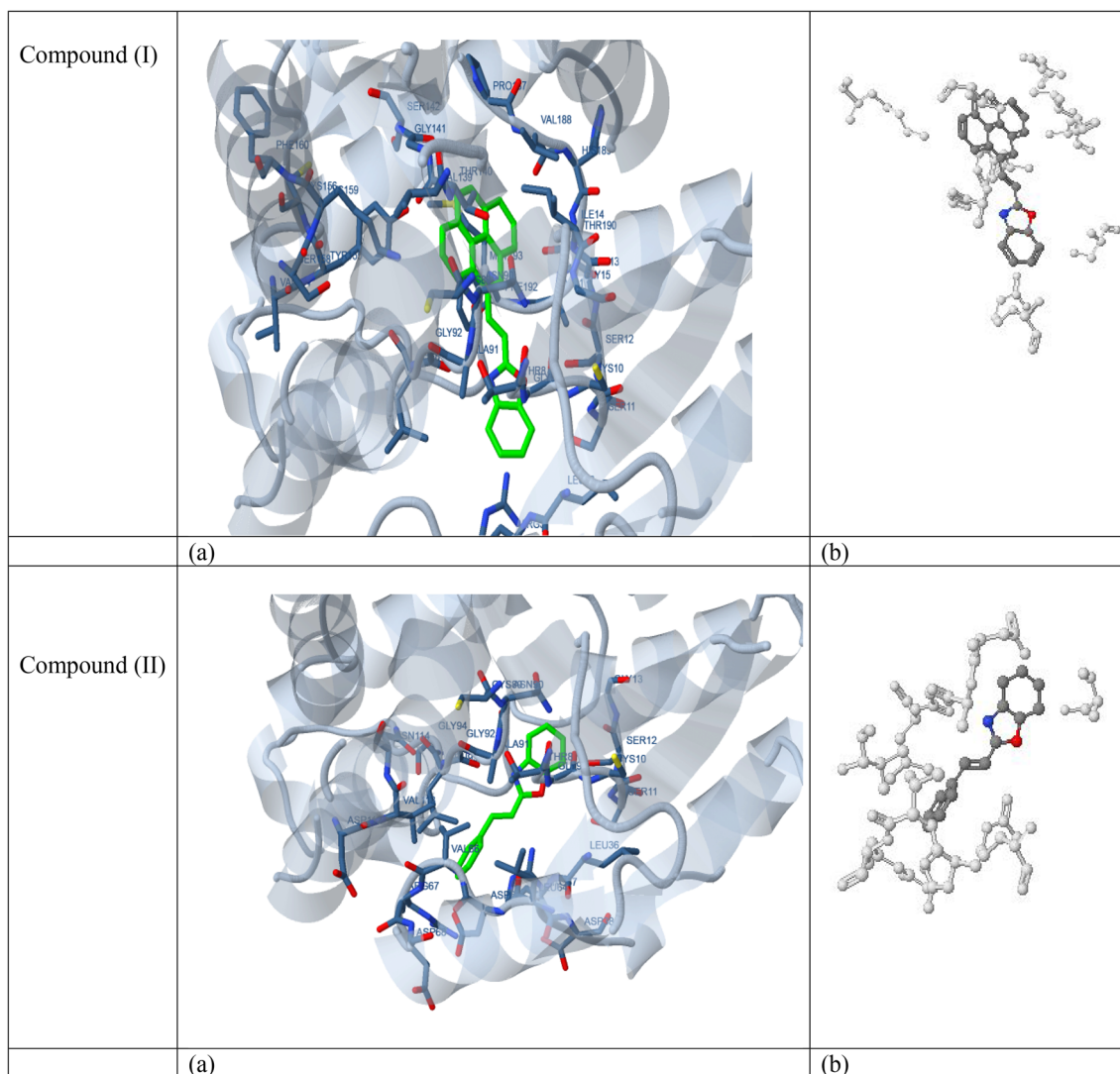
Fig. 12 Interaction of the benzo[d]oxazole compounds (I) and (II) with the receptor of the breast cancer mutant 3hb5-oxidoreductase (green in (**a**) and grey in (**b**))

receptor of the breast cancer mutant 3hb5-oxidoreductase in this study. The findings revealed a potential arrangement of benzo[d]oxazole derivatives. As well as the 3hb5 receptor. As illustrated in Fig. 12, the docking research reveals a positive contact between benzo[d]oxazole derivatives and the receptor (3hb5), and the observed energy is documented in Table 10.

As illustrated in Fig. 13, the HB curve demonstrates that benzo[d]oxazole derivatives attach to proteins via hydrogen bond interactions, and decomposed interaction energies exist among benzo[d]oxazole derivatives with the 3hb5 receptor.

Table 10 Docking measurements of benzo[d]oxazole compounds (I, II) with the receptor of breast cancer mutant 3hb5-oxidoreductase provided energy data

Compound No	Est. Free Energy of Binding (kcal/mol)	Est. inhibition constant (K_i) (µM)	vdW + bond + desolv-energy (kcal/mol)	Electrostatic Energy (kcal/mol)	Total intercooling Energy (kcal/mol)	Interact surface
(I)	− 9.00	250.82	− 9.63	+ 0.04	− 9.59	884.044
(II)	− 6.79	10.55	− 7.30	− 0.08	− 7.38	635.696

Interactions

11: SER
14: ILE
37: ARG
91: ALA
92: GLY
140: THR
159: LYS
188: VAL
190: THR
192: PHE

Compound (I)

Interactions

12: SER
37: ARG
65: ASP
66: VAL
67: ARG
90: ASN
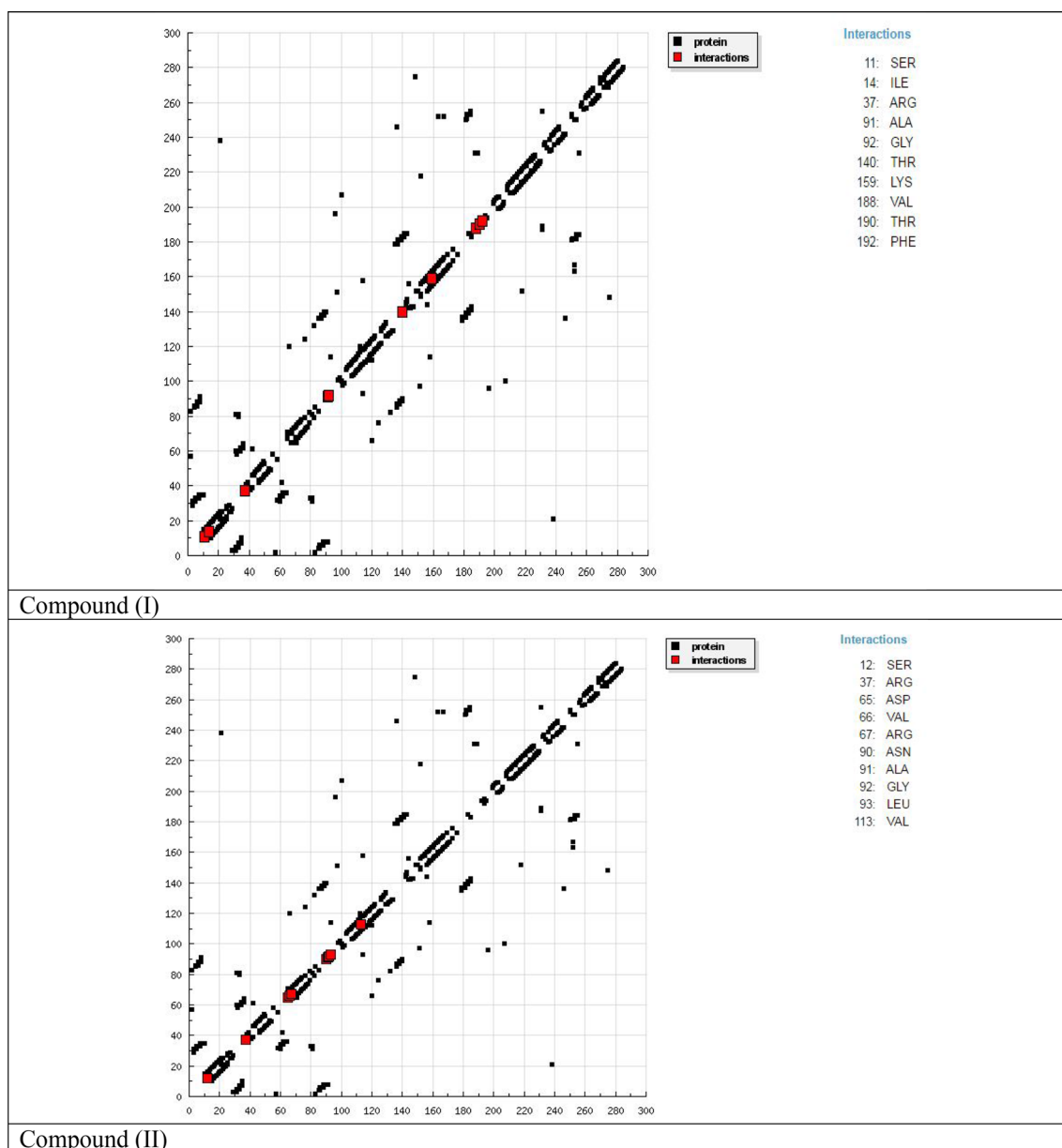91: ALA
92: GLY
93: LEU
113: VAL

Compound (II)

Fig. 13 HB plot of interactions between benzo[d]oxazole compounds (I) and (II) and the 3hb5-oxidoreductase receptor of a breast cancer mutant

3.9 Corrosion Mechanism

For all approaches, the percent IE varies depending on the type of adsorpting inhibitors on C-steel, surface conditions, metal nature, and concentration. The following are the results of corrosion with inhibitors (I, II): With a larger inhibitor concentration, the rate and i_{corr} are reduced. The desorption of the inhibitor was caused by a decrease in the percent IE as the temperature rose. It was discovered that the type of adsorption is determined by the C-capacity steel's to directly interact with the ring π-electron clouds.

The order of decreasing compound inhibition efficiency from all methods used is compound (I) > compound (II). Compound (I) has good inhibition ability because of: I its larger molecular size (347), which may allow for a bigger molecule area and improved surface coverage; and (ii) its adsorption via two active centres (1-O, and 1-N atoms). Compound (II) has a lower inhibitory efficacy than compound (I) due to its smaller molecular size (221) and adsorption through two active sites (1-O, and 1-N atoms).

4 Conclusion

The data from experimental and theoretical Studies were in excellent agreement, %IE of these assembled is compound (I) > compound (II). The double layer capacitances decrease when the inhibitor is introduced to the blank solution. EFM is thus a non-destructive method of measurement. Researchers employed a quantum chemical approach based on density functional theory to better understand the link between the protection adequacy and the molecular structure of benzo[d]oxazole derivatives (DFT).

Declarations

Conflict of interest The authors declare that there is no conflict of interest.

References

1. Ahamad RP, Quraishi MA (2010) Thermodynamic, electrochemical and quantum chemical investigation of some schiff bases as corrosion inhibitors for mild steel in hydrochloric acid solutions. Corros Sci 52(3):933–942

2. Bouklah M, Hammouti B, Benkaddour M, Benhadda T (2005) J Appl Electrochem 35:1095–1101

3. Fiala A, Chibani A, Darchen A, Boulkamh A, Djebbar K (2007) Investigations of the inhibition of copper corrosion in nitric acid solutions by ketene dithioacetal derivatives. Appl Surf Sci 253:9347–9356

4. Foudaa AS, Al-Sarawyb AA, El-Katorib EE (2006) Pyrazolone derivatives as corrosion inhibitors for C-steel in hydrochloric acid solution. Desalination 201(1–3):1–13

5. Ishtiaque Ahamad, Rajendra Prasad, Quraishi MA (2010) Adsorption and inhibitive properties of some new mannich bases of Isatin derivatives on corrosion of mild steel in acidic media. Corros Sci 52(4):1472–1481

6. Yadav DK, Maiti B, Quraishi MA (2010) Electrochemical and quantum chemical studies of 3,4-dihydropyrimidin-2(1H)-ones as corrosion inhibitors for mild steel in hydrochloric acid solution. Corros Sci 52:3586–3598

7. Salem Edrah, Hasan SK (2010) Studies on thiourea derivatives as corrosion inhibitor for aluminum in sodium hydroxide solution. J Appl Sci Res 6(8):1045–1049

8. Tan YJ, Bailey S, Kinsella B (1996) The monitoring of the formation and destruction of corrosion inhibitor films using electrochemical noise analysis (ENA). Corros Sci 38(10):1681–1695

9. Dahmani M, Et-Touhami A, Al-Deyab SS, Hammouti B, Bouyanzer A (2010) Corrosion inhibition of C38 steel in 1 M HCl: A comparative study of black pepper extract and its isolated piperine. Int J Electrochem Sci 5:1060–1069

10. Mohamad AB, Kadhum AAH, Al-Amiery AA, Ying LC, Musa AY (2014) Synergistic of a coumarin derivative with potassium iodide on the corrosion inhibition of aluminum alloy in 1.0 M H2SO4. Metals Mater Int 20:459–467

11. Sherif EM, Park SM (2012) Corrosion behavior of copper in 050 m hydrochloric acid pickling solutions and its inhibition by 3-Amino-1,2,4-triazole and 3-Amino-5-mercapto-1,2,4-triazole. Int J Electrochem Sci 7(3):1884–1897

12. Sherif EM, Park SM (2015) Corrosion inhibition of carbon steel in aggressive acidic media with 1-(2-(4-chlorophenyl)-2-oxoethyl)pyridazinium bromide. J Mol Liq 211:1000–1008

13. Abd El-Maksoud SA, Fouda AS (2005) Some pyridine derivatives as corrosion inhibitors for carbon steel in acidic mediu. Mater Chem Phys 93(1):84–90. https://doi.org/10.1016/j.matchemphys.2005.02.020

14. Srikanth AP, Sunitha TG, Raman V, Nanjundan S, Rajendran N (2007) Synthesis, characterization and corrosion protection properties of poly(N-(acryloyloxymethyl) benzotriazole- coglycidyl methacrylate) coatings on mild steel. Mater Chem Phys 103(2):241–247. https://doi.org/10.1016/j.matchemphys.2007.02.021

15. Bouklah M, Attayibat A, Hammouti B, Ramdani A, Radi S, Benkaddour M (2005) Pyridine–pyrazole compound as inhibitor for steel in 1 M HCl. Appl Surf Sci 240(1–4):341–348

16. Rogers RD, Seddon KR (2003) Ionic liquids-solvents of the future? J Sci 302:792–793. https://doi.org/10.1126/science.1090313

17. Jain N, Kumar A, Chauhan S, Chauhan SMS (2004) Chemical and biochemical transformations in ionic liquids. Tetrahedron 61(5):1015–1560. https://doi.org/10.1016/j.tet.2004.10.070

18. Wilkes JS (2002) A short history of ionic liquids—from molten salts to neoteric solvent. J Green Chem 4:73

19. Ngo HL, Le Compte K, Hargens L, McEwen AB (2011) Analysis of evaporation and thermal decomposition of ionic liquids by thermogravimetrical analysis at ambient pressure and high vacuum. Green chem. https://doi.org/10.15495/EPub_UBT_00004728

20. Ngo HL, Le Compte K, Hargens L, McEwen AB, Thermochim J (2000) Thermal properties of imidazolium ionic liquids. Thermochim Acta 357–358(5):97–102. https://doi.org/10.1016/S0040-6031(00)00373-7

21. Bonhôte P, Dias A-P, Papageorgiou N, Kalyanasundaram K, Gratzel M (1996) Hydrophobic, highly conductive Ambient-temperature molten SALTS. Inorg Chem 35:1168

22. Forsyth SA, Pringle JM, MacFarlane DR (2004) Ionic Liquids—An Overview. Aust J Chem 57(2):113–119

23. Endres F, Abedin SZE (2006) Air and water stable ionic liquids in physical chemistry. Phys Chem Chem Phys 8:2101–2116

24. Endres F, El Abedin SZ, Matter S (2006) Air and water stable ionic liquids in physical chemistry. Phys Chem Chem Phys 8:2101

25. Ibrahim MAM, Messali M (2011) Corrosion inhibition of carbon steel in aggressive acidic media with 1-(2-(4-chlorophenyl)-2-oxoethyl) pyridazinium bromide. Phys Chem 76:14

26. Al-Ghamdi FA, Messali M, Ahmed SA (2011) Corrosion inhibition of carbon steel in aggressive acidic media with 1-(2-(4-chlorophenyl)-2-oxoethyl)pyridazinium bromide. J Mater Environ Sci 2:215

27. Hagiwara R, Ito Y (2000) Room temperature ionic liquids of alkylimidazolium cations and fluoroanions. J Fluor Chem. https://doi.org/10.1016/S0022-1139(99)00267-5

28. Messali M, Ahmed SA (2011) A green microwave-assisted synthesis of new pyridazinium-based ionic liquids as an environmentally friendly alternative. Green Sustain Chem. https://doi.org/10.4236/gsc.2011.13012

29. Quraishi MA, Rafiquee MZA, Khan S, Saxena N (2007) Corrosion inhibition of aluminium in acid solutions by some

imidazoline derivatives, J. Electroch, Appl. https://doi.org/10.1007/s10800-007-9379-0

30. Ibrahim MAM, Messali M, Moussa Z, Alzahrani AY, Alamry SN (2011) Corrosion inhibition of carbon steel by imidazolium and pyridinium cations ionic liquids in acidic environment. Electrochim Acta 29:375

31. Messali M (2011) synthesis, characterization and comparative study of new pyridazinium-based ionic liquids derivatives towards corrosion of mild steel in acidic environment. J Mater Environ Sci 2:174

32. Ibrahim MAM, Messali M, Moussa Z, Alzahrani AY, Alamry SN (2011) Experimental and theoretical studies on some selected ionic liquids with different cations/anions as corrosion inhibitors for mild steel in acidic medium. J Electrochim Acta 29:375

33. Messali M (2011) A green microwave-assisted synthesis, characterization and comparative study of new pyridazinium-based ionic liquids derivatives towards corrosion of mild steel in in acidic environment. J Mater Environ Sci 2:174

34. Palomar ME, Olivares-Xometl CO, Likhanova NV, Pérez-Nava JB (2011) Corrosion inhibition of carbon steel by imidazolium and pyridinium cations ionic liquids in acidic environment. Port Electrochim Acta 14:211

35. Ben Aoun S (2013) Gravimetric and temperature effect studies of a novel imidazolium-based ionic liquid as a corrosion inhibitor for carbon steel in molar hydrochloric acid. Der Pharma Chem 5:294

36. Sangeetha M, Rajendran S, Sathiyabama J, Krishnaveni A, Shanthy P, Manimaran N, Shyamaladevi B (2011) corrosion inhibition by an aqueous extract of phyllanthus amarus. Port Electrochim Acta. https://doi.org/10.4152/pea.201106429

37. Rosliza R, Senin HB, Wan Nik WB (2008) Electrochemical properties and corrosion inhibition of AA6061 in tropical seawater. J Coll Surf 312:185

38. Pinto GM, Nayak J, Nityananda Shetty A (2011) Corrosion inhibition of carbon steel in aggressive acidic media with 1-(2-(4-chlorophenyl)-2-oxoethyl)pyridazinium bromide. J Mater Chem Phys 125:628

39. Messali M, Bousskri A, Anejjar A, Salghi R, Hammouti B (2015) Electrochemical Studies of 1-(2-(4-nitrophenyl)-2-oxoethyl)pyridazinium bromide, On Carbon Steel corrosion in hydrochloric acid medium. Int J Electrochem Sci 10:4551

40. Messaadia L, El Mouden OID, Anejjar A, Messali M, Salghi R, Benali O, Hammouti B, Cherkaoui O, Lallam A (2015) Adsorption and corrosion inhibition of new synthesized Pyridazinium-Based Ionic Liquid on Carbon steel in 05 M H2SO. J Mater Environ Sci 6:606

41. Dawood H, Alshemary K, Sabeeh N (2022) Microstructure thermal and mechanical properties of friction stir welded 6061 aluminum alloy with 10% SiCp reinforcement. Egypt J Chem. https://doi.org/10.21608/ejchem.2021.110858.5053

42. Abdel Hamed RS, Qureshi MT, Abdallah M (2021) Cathodic delamination of polymer coatings from metals mechanism and prevention methods a review. Int J Corros Scale Inhib 10(1):68–79

43. Halgren TA (1998) Merck molecular force field I Basis, form, scope, parameterization, and performance of MMFF94. J Computat Chem 17:490

44. Morris GM, Goodsell DS (1998) Automated docking using a Lamarckian genetic algorithm and an empirical binding free energy function. J Comput Chem 19:1639

45. Raghavendra NM, Ramakrishna K, Sirisha V, Divya P (2013) Computer aided discovery of potential anti-inflammatory (s)-naproxen analogs as COX-2 inhibitors. J Med Chem 9:553

46. Gadow HS, Farghaly TA, Eldesoky AM (2022) In an Acidic Environment, Perimidin-10-one Derivatives were Evaluated as Potential Copper Corrosion Inhibitors (Experimental and Theoretical Examinations). J Bio and Tribo Corrosion 8:51

47. Wiercinska AN, Dalmata G (2006) Adsorption of N, N′-dimethylthiourea at a mercury/aqueous solution of NaClO4 interface; dependence on the supporting electrolyte concentration. J Electrochim Acta 51:6179

48. Yurt A, Balaban A, Kandemir SU, Bereket G, Erk B (2004) Investigation on some Schiff bases as HCl corrosion inhibitors for carbon steel. J Mater Chem Phys 85:420

49. Etre AY (2006) Khillah extract as inhibitor for acid corrosion of SX 316 steel. J Appl Surf Sci 252:8521

50. Lorenz WJ, Mansfeld F (1981) Determination of corrosion rates by electrochemical DC and AC methods. J Corros Sci 21:647

51. Putilova IN, Balezin SA, Barannik VP (1960) Metallic Corrosion Inhibitors Pergamon. Press, New York

52. Al-Neami KK, Mohamed AK, Kenawy IM, Fouda AS (1995) Inhibition of the corrosion of iron by oxygen and nitrogen containing compounds. J Monatsh Chem 126:369

53. Noor EA (2007) Temperature effects on the corrosion inhibition of mild steel in acidic solutions by aqueous extract of fenugreek leaves. Int J Electrochem Sci 2:996

54. Marsh J (1988) Advanced Organic Chemistry, 3rd edn. Wiley, New Delhi

55. Martinez S, Stern I (2002) Thermodynamic characterization of metal dissolution and inhibitor adsorption processes in the low carbon steel/mimosa tannin/sulfuric acid system. J Appl Surf Sci 199:83

56. Al-Khaldi MA, Al-qahtani KY (2013) Corrosion inhibition of steel by Coriander extracts in hydrochloric acid solution. J Mater Environ Sci 4(5):593

57. Schltze JW, Wippermann K (1987) Inhibition of electrode processes on copper by AHT in acid solutions. J Electrochim Acta 32:823

58. Silverman DC, Carrico JE (1988) Electrochemical impedance technique—a practical tool for corrosion prediction. J Corrosion 44:280

59. Macdonald DD, Mckubre MCH (1982) Impedance measurements in electrochemical systems. In: Bockris JO'M, Conway BE, White RE (eds) Modern Aspects of Electrochemistry. Plenum Press, New York

60. Mansfeld F (1981) Recording and analysis of AC impedance data for corrosion studies. J Corros 36:301

61. Gabrielli C (1980) Identification of Electrochemical processes by Frequency Response Analysis. Solarton Instrumentation Group, California

62. El Achouri M, Kertit S, Gouttaya HM, Nciri B, Bensouda Y, Perez L, Infante MR, Elkacemi K (2001) Corrosion inhibition of iron in 1 M HCl by some gemini surfactants in the series of alkanediyl-α, ω-bis-(dimethyl tetradecyl ammonium bromide). J Prog Org Coat 43:267

63. Anejjar A, Zarrouk A, Salghi R, Zarrok H, Ben Hmamou D, Hammouti B, Elmahi B, Al-Deyab SS (2013) Studies on the inhibitive effect of the ammonium Iron (II) sulphate on the corrosion of carbon steel in HCl solution. J Mater Environ Sci. 4:583

64. Mertens SF, Xhoffer C, Decooman BC, Temmerman E (1997) Short-term deterioration of polymer-coated 55% Al-Zn—part 1: behavior of thin polymer films. J Corros 53:381

65. Trowsdate AJ, Noble B, Haris SJ, Gibbins ISR, Thomson GE, Wood GC (1996) The influence of silicon carbide reinforcement on the pitting behaviour of aluminium. J Corros Sci 38:177

66. Reis FM, de Melo HG, Costa I (2006) EIS investigation on Al 5052 alloy surface preparation for self-assembling monolayer. J. Electrochem. Acta 51:1780

67. Lagrenée M, Mernari B, Bouanis M, Traisnel M, Bentiss F (2002) Study of the mechanism and inhibiting efficiency of 3, 5-bis (4-methylthiophenyl)-4H-1, 2, 4-triazole on mild steel corrosion in acidic media. J Corros Sci 44:573

68. McCafferty E, Hackerman N (1972) Kinetics of iron corrosion in concentrated acidic chloride solutions. J Electrochem Soc 119:999

69. Ma H, Chen S, Niu L, Zhao S, Li S, Li D (2002) Inhibition of copper corrosion by several Schiff bases in aerated halide solutions. J Appl Electrochem 32:65

70. Kuş E, Mansfeld F (2006) An evaluation of the electrochemical frequency modulation (EFM) technique. J Corros Sci 48:965

71. Tan B, Zhang S, Cao X, Fu A, Guo L, Marzouki R, Li W (2022) Insight into the anti-corrosion performance of two food flavors as eco-friendly and ultra-high performance inhibitors for copper in sulfuric acid medium. J Colloid Interface Sci 609:838–851

72. Idir B, Kerkouche F (2018) Experimental and theoretical studies on corrosion inhibition performance of phenanthroline for cast iron in acid solution. J electrochem sci technol 9:260–275

73. Caigman GA, Metcalf SK, Holt EM (2000) Thiophene substituted dihydropyridines. J Chem Cryst 30:415

74. Samie F, Tidblad J, Kucera V, Leygraf C (2005) Atmospheric corrosion effects of HNO3—method development and results on laboratory-exposed copper. J Atmospheric Environ 39:7362

75. Prabhu RA, Venkatesha TV, Shanbhag AV, Kulkarni GM, Kalkhambkar RG (2008) Inhibition effects of some schiff's bases on the corrosion of mild steel in hydrochloric acid solution. J Corros Sci 50:3356

76. Moretti G, Quartanone G, Tassan A, Zingales A (1994) Inhibition of mild steel corrosion in 1N sulphuric acid through indole. J Wekst Korros 45:641

77. Samie F, Tidblad J, Kucera V, Leygraf C (2006) Atmospheric corrosion effects of HNO3—Influence of concentration and air velocity on laboratory-exposed copper. J Atmospheric Environ 40:3631

78. Lukovits I, Palfi K, Bako I, Kalman E (1997) LKP model of the inhibition mechanism of thiourea compounds. J Corrosion 53:915

79. Zhao P, Liang Q, Y Li (2005) Electrochemical, SEM/EDS and quantum chemical study of phthalocyanines as corrosion inhibitors for mild steel in 1 mol/l HCl. J Appl Surf Sci 252:1596

80. Mohamed GG, El-Sherif AA, Saad MA, El-Sawy SEA, Morgan ShM (2016) Mixed-ligand complex formation of tenoxicam drug with some transition metal ions in presence of valine: synthesis, characterization, molecular docking. J Mol Liq 223:1311

81. Refaat HM, El-Badway HA, Morgan ShM (2016) Molecular docking, geometrical structure, potentiometric and thermodynamic studies of moxifloxacin and its metal complexes. J Mol Liq 220:802